



Insight of platinum poisoning Cu/SAPO-34 during NH₃-SCR and its promotion on catalysts regeneration after hydrothermal treatment

Tie Yu^{a,b,d}, Minhong Xu^{a,1}, Yu Huang^a, Jianqiang Wang^a, Jun Wang^{a,*}, Liangfang Lv^a, Gongshin Qi^{d,**}, Wei Li^d, Meiqing Shen^{a,c}

^a Key Laboratory for Green Chemical Technology of State Education Ministry, School of Chemical Engineering & Technology, Tianjin University, Tianjin 300072, PR China

^b State Key Laboratory of Catalysis, Dalian Institute of Chemical Physics, Chinese Academy of Sciences, Zhongshan Road 457, Dalian 116023, PR China

^c State Key Laboratory of Engines, Tianjin University, Tianjin 300072, PR China

^d General Motors Global Research and Development, Chemical Sciences and Materials Systems Lab, 3500 Mound Road, Warren, MI 48090, USA

ARTICLE INFO

Article history:

Received 4 August 2016

Received in revised form

21 November 2016

Accepted 3 December 2016

Available online 5 December 2016

Keywords:

NH₃-SCR

SAPO-34

Hydrothermal treatment

Regeneration

Platinum

ABSTRACT

This study mainly focused on selective catalytic reduction of air pollutants NO_x by ammonia (NH₃-SCR), and a series of Pt impregnated Cu/SAPO-34 (homemade) samples were employed to elucidate its negative impact on DeNO_x activity and hydrothermal treatment's acceleration on NH₃-SCR activity resurgence. Firstly, XRD, NH₃-TPD and DRIFTS were performed to examine platinum interaction with zeolites structure and contribution to acidity. Then, Pt inhibition on NH₃-SCR activity was evaluated and its impact on reaction network, including ammonia oxidation, NO oxidation and NO + NH₃, was concluded based on gas switching tests. H₂-TPR and EPR further reflected various Cu species coordination and redox capacity variation caused by platinum doping. It was intriguing to find out that the further hydrothermal treatment benefited rejuvenation of Pt-poisoned Cu/SAPO-34 and even activity enhancement from Pt presence under the condition of zeolites structure integrity. Hydrothermal treatment induced platinum sintering and STEM illustrated platinum species combined with copper oxides and generated oxo-complexes, weakening ammonia oxidation. And Pt presence promoted copper oxides further dispersion during hydrothermal treatment. Finally, platinum poisoning on Cu/SAPO-34 and its regeneration after hydrothermal treatment were concluded to indicate their application potential.

© 2016 Elsevier B.V. All rights reserved.

1. Introduction

Selective Catalytic Reduction of NO_x by ammonia (NH₃-SCR) is an efficient technology to eliminate the hazardous nitrogen oxides from diesel vehicle [1–5]. Until now there are various kinds of NH₃-SCR catalysts invented, such as: noble metal catalysts [2,6], oxides catalysts [7–10] and zeolites catalysts [11–15]. Nevertheless, only the zeolites NH₃-SCR catalysts research gets more and more practical attention due to their wider temperature window and higher N₂ selectivity during DeNO_x process. Since 2009, the appearance of NH₃-SCR reports over Cu/SAPO-34 catalyst has

caught a great attention because this catalyst showed much better SCR activity and hydrothermal stability compared with commercialized Cu/ZSM-5 catalyst [16–20]. The following massive studies found that Cu/chabazite (CHA), including SAPO-34 and SSZ-13, both performed superior SCR activity and framework hydrothermal stability after 750 °C for 12 h due to their unique small pore structure [13,16,21–23]. Furthermore, lots of studies have been conducted to confirm the appropriate preparation methods, the structure-activity relation and reaction mechanism over Cu/CHA, which proved the isolated Cu²⁺ species coordinated with frameworks are the NH₃-SCR active sites [24–30]. Ion-exchange and one-pot methods benefited more Cu²⁺ species generation than impregnated way, and aged Cu/SAPO-34 presented better NO_x conversion due to the transition from CuO species to Cu²⁺ species in presence of water during hydrothermal treatment.

Except the hydrothermal stability, sulfur and noble metal resistance of Cu/CHA catalysts should also be considered during their application, since SO₂ from exhaust gas and noble metal such as platinum from upstream oxidation catalysts could poison SCR

* Corresponding author at: School of Chemical Engineering and Technology, Tianjin University, 92 Weijin Road, Nankai District, Tianjin 300072, China. Tel./fax: +86 22 27892301.

** Corresponding author at: Chemical Sciences & Materials Systems Laboratory, General Motors Global R&D, Warren, MI, USA.

E-mail addresses: wangjun@tju.edu.cn (J. Wang), Gongshin.qi@gm.com (G. Qi).

¹ Co-first author.

catalyst. And in this study platinum (Pt) poisoning on Cu/SAPO-34 catalysts and their regeneration will be investigated overall to examine the practicability. For Cu-based zeolites catalysts, Ford Motor Company reported platinum group metal (PGM) from upstream volatilized and deposited on downstream SCR catalysts up to 850 °C, and this contamination caused decreased NO_x conversion and excessive N₂O formation. The palladium actually showed less impact on SCR activity, while platinum greatly influenced NO_x conversion efficiency [31,32]. Based on these results, Cummins Inc. further proved the platinum poisoning benefited NH₃ oxidation, which generated more N₂O during 300–350 °C and decreased NO_x conversion at high temperature. And they also explored the rejuvenation of Pt-contained Cu-zeolites under the thermal treatment at 700 °C without structure damage. It was considered Pt contamination in Cu-zeolites could be partially recovered due to platinum sintering [33]. Recently, Lezcano-Gonzalez and et al. studied series pollutants (Pt, Zn, Ca and P) to Cu/SSZ-13 catalysts during SCR process, and platinum presented the same poisoning effect on N₂ selectivity and NO_x conversion decrease, which was predicted to be due to Pt species oxidation ability but not its modification on support structure or active Cu²⁺ sites [34]. However, there is still no systematically research about platinum influence on acidity, Cu²⁺ sites and reaction mechanism over Cu/SAPO-34 catalysts during NH₃-SCR process, and regeneration of Pt-poisoned Cu/SAPO-34 in presence of steam will be initially considered due to its existence in exhaust gases.

In this study, a series of Pt impregnated Cu/SAPO-34 samples (homemade) were employed to elucidate its poisoning impact on catalysts and NH₃-SCR performance. XRD, NH₃-TPD and DRIFTS were firstly performed to check platinum influence on zeolites structure and acidity. Then, Pt inhibition on NH₃-SCR activity was evaluated and its impact on reaction network was concluded based on gas switching tests. H₂-TPR and EPR reflected Cu species variation caused by platinum and the further hydrothermal treatment benefited rejuvenation of Pt-poisoned Cu/SAPO-34. STEM illustrated platinum coordination with copper oxides before and after this treatment. Finally, the platinum poisoning on Cu/SAPO-34 catalysts and their regeneration after hydrothermal treatment was concluded to explain the application potential.

2. Experimental

2.1. Preparation of catalysts

The SAPO-34 supports here were prepared with the mole composition of 0.2 Morpholine (MA): 0.1 Al₂O₃: 0.1 P₂O₅: 0.1 SiO₂: 6.5 H₂O through hydrothermal method. The detailed procedure was the same with our previous reports [35,36]. And silica sol, 85% phosphoric acid and pseudoboehmite were the sources of skeleton Si, P, and Al in SAPO-34 molecular sieves, respectively. The SAPO-34 composition was obtained from X-ray fluorescence spectrometer (XRF) and abbreviated as Si_{0.13}Po_{0.36}Al_{0.51}.

Cu/SAPO-34 catalysts were prepared through ion-exchange method of two steps. Firstly, NH₄-SAPO-34 was synthesized by exchanging H/SAPO-34 in ammonium nitrate solution at 80 °C. Then Cu/SAPO-34 was obtained by exchanging NH₄-SAPO-34 in copper sulfate solution. After each ion-exchange procedure, the slurry was filtered, washed and dried at 100 °C for 16 h in oven. The dried Cu/SAPO-34 was further calcined in muffle furnace for 4 h at 550 °C. For Pt-containing samples, Pt was loaded on Cu/SAPO-34 precursor by wet impregnation using Pt (NO₃)₂ solution before the precursor was calcined. The Cu and Pt loadings were examined by ICP and these results were shown in Table 1. The Cu zeolites catalyst was named as Cu/Pt loading for short.

Table 1

Composition of all catalysts.

Sample	Pt loading (wt%)	Cu loading (wt%)
Cu/SAPO-34 (Cu)	0	1.7
Cu-Pt0.1/SAPO-34 (Cu/P01)	0.1	1.7
Cu-Pt0.5/SAPO-34 (Cu/P05)	0.5	1.7
Cu-Pt1/SAPO-34 (Cu/P10)	1	1.7
Pt1/SAPO-34 (P10)	1	1.7

To investigate the hydrothermal stability and regeneration of Pt poisoned Cu/SAPO-34 samples, all catalysts were treated at 750 °C in 1 L min⁻¹ air with 10% H₂O for 12 h. And fresh and aged catalysts were distinguished by the suffix of (–F) or (–A). In order to further investigate aging temperature influence on catalytic activity rejuvenation, Cu/P10 and P10 samples were chosen to be treated also at 850 °C for 6 h.

2.2. Bulk characterization

XRD patterns were conducted over X'Pert Pro diffractometer operating at 40 kV and 40 mA with nickel-filtered Cu Kα radiation ($\lambda = 1.5418 \text{ \AA}$) during $5^\circ < 2\theta < 50^\circ$ with 0.02° step size. Temperature programmed desorption tests using NH₃ as probe (NH₃-TPD) were conducted to examine sample acidity at 80 °C. The catalysts were pretreated at 500 °C for 10 min in 5% (vol) O₂ before the experiments, and then cooled down to 80 °C under N₂. NH₃ adsorption was conducted with 500 ppm NH₃/N₂ until the outlet NH₃ concentration kept stable. Then, N₂ was utilized to purge any weakly absorbed NH₃ on catalysts. Finally, the temperature was raised from 80 °C to 600 °C with a ramping rate of 10 °C/min.

Ex-situ DRIFTS (Diffuse reflectance infrared Fourier transform spectra) were performed on Nicolet 6700 spectrometer equipped a MCT detector and a high temperature reaction chamber with ZnSe windows, which was connected to a gas-dosing system. And the tests were measured at 200 °C and KBr spectrum under the same condition was used as the background. The testing spectra range was 4000–650 cm⁻¹ with a resolution of 2 cm⁻¹.

Hydrogen Temperature Programmed Reduction (TPR) experiments were conducted in a U-shaped tubular quartz reactor. Firstly, the sample was pre-oxidized at 500 °C under a 30 mL min⁻¹ 2% O₂/N₂ and maintained for 30 min. During the temperature programmed reduction process, the temperature was elevated to 900 °C under 15 mL min⁻¹ 5% H₂/N₂ at a 5 °C min⁻¹ ramping rate. The thermal conductivity detector was employed to quantify hydrogen consumption.

The Electron Paramagnetic Resonance (EPR) spectra, to examine the location and coordination of isolated copper species, were performed on a Bruker ESP320 spectrometer. Meanwhile, the corresponding Bruker ESP320E software and Bruker program were utilized for data analysis. The EPR spectra were collected at atmospheric pressure and room temperature. And before the EPR tests, the Cu/SAPO-34 catalysts were vacuumed under $4.0 \times 10^{-4} \text{ Pa}$ for an hour at 120 °C.

The X-ray photoelectron spectroscopy (XPS) experiment was carried out on a PHI-1600 ESCA system by employing an Mg Kα source operating at 250 W. The electron takeoff angle was 45° with respect to the sample surface. The binding energy was calibrated internally by the carbon deposit C 1s binding energy (BE) at 284.8 eV.

High resolution transmission electron microscopy (HRTEM) and energy-filtered transmission electron microscopy (EFTEM) with an energy resolution of 0.3–2 eV, using the Gatan imaging filter (GIF 200) attached to the transmission (TEM) Tecnai G2F20 operated at 200 keV, were conducted to characterize the Pt particles and Pt-copper species location in Cu/SAPO-34 catalysts. Point analy-

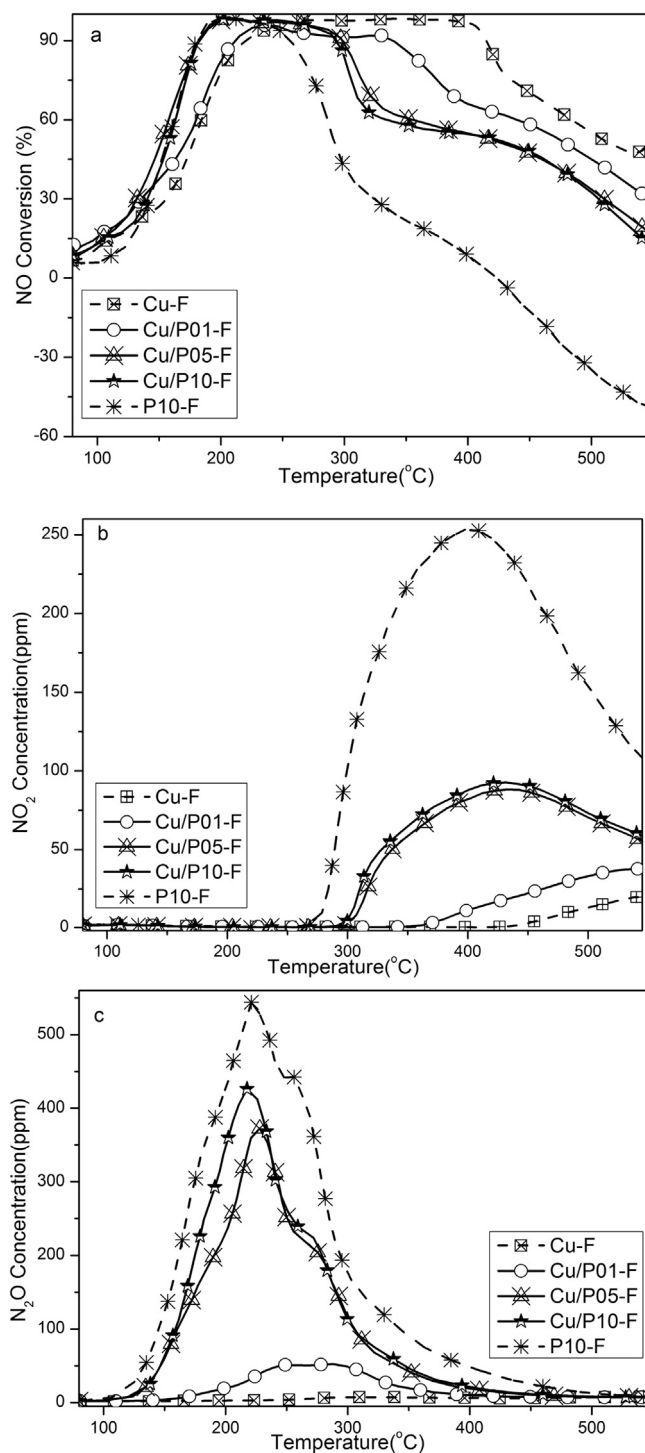


Fig. 1. NH₃-SCR performance as a function of temperature. (a) NO conversion; (b) NO₂ and (c) N₂O generation. The feed contained 500 ppm NH₃, 500 ppm NO, 5% O₂, N₂ was the balance. The flow rate and space velocity in all experiment were controlled at 500 mL min⁻¹ and 300,000 h⁻¹.

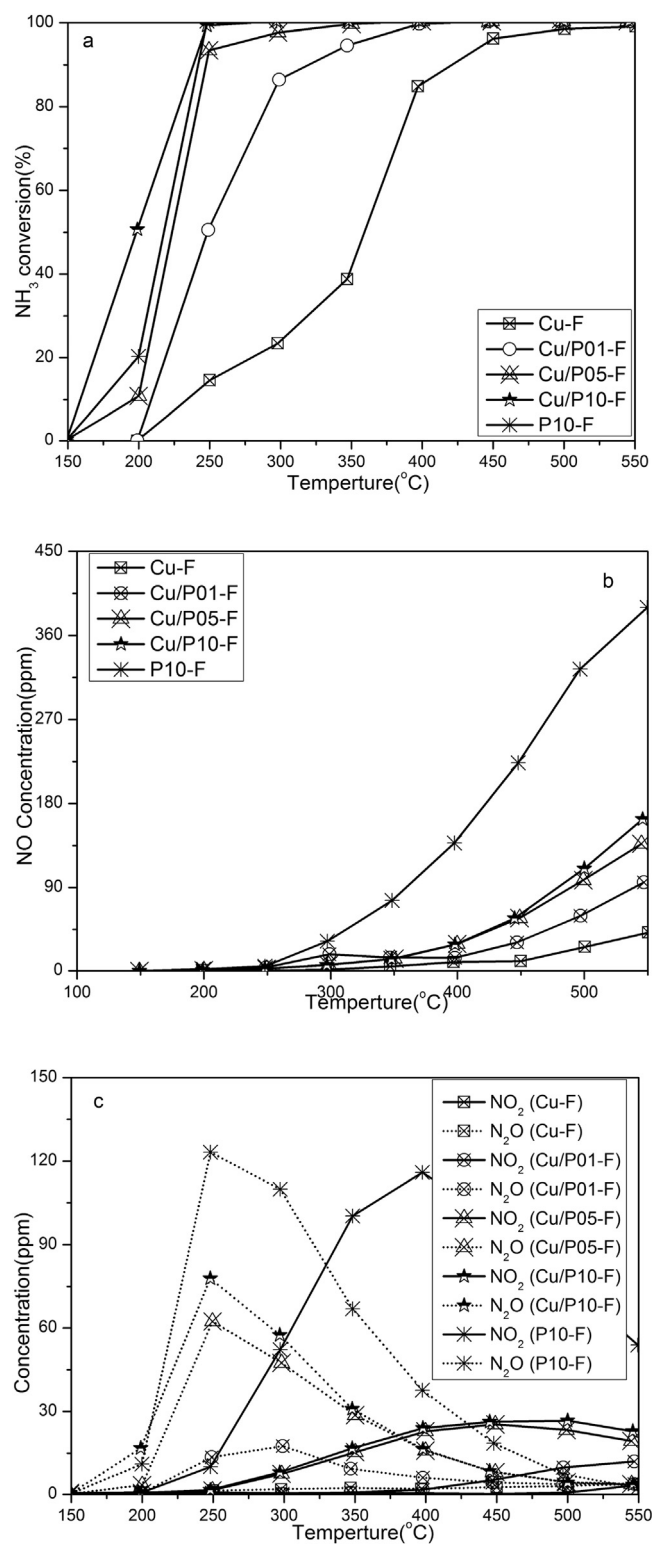


Fig. 2. NH₃ oxidation results over Cu/SAPO-34 catalysts. (a) NH₃ conversion; (b) NO concentration; (c) NO₂, N₂O concentrations. The inlets consisted of 500 ppm NH₃, 5% O₂ with N₂ as the balance. The flow rate and volume hourly space velocity in all experiment were controlled at 500 mL min⁻¹ and 300,000 h⁻¹.

ses were made in the nano-probe mode with the electron probe of a few nanometers in diameters. Before imaging, the powder was dissolved in anhydrous ethanol and lightly dusted onto 230 mesh Cu grids coated with ultrathin carbon.

2.3. Catalytic performance

NH₃-SCR activity was conducted in a quartz reactor using 100 mg samples (60–80 mesh) mixed with 900 mg quartz (60–80 mesh) under atmospheric pressure. The catalysts bed

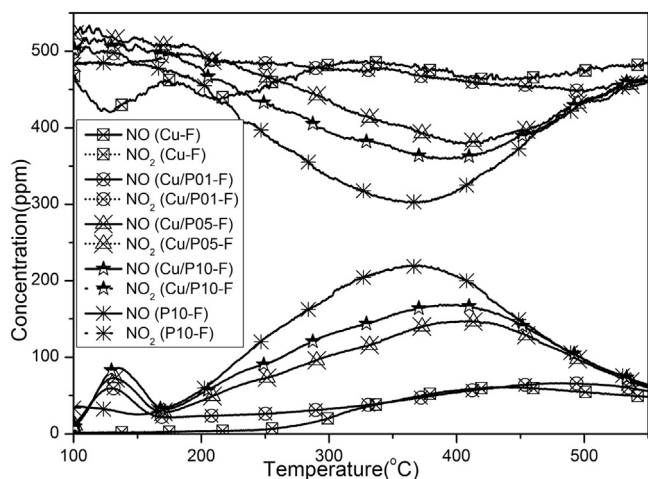


Fig. 3. NO oxidation results over Cu/SAPO-34 catalysts. The inlets consisted of 500 ppm NO, 5% O₂ with N₂ as the balance. The flow rate and volume hourly space velocity in all experiment were controlled at 500 mL min⁻¹ and 300,000 h⁻¹.

was sealed in the tube by quartz wool. And the temperature was controlled by a type K thermocouple inserted into the center of the catalyst bed. The inlets flow rates and space velocity were controlled at 500 mL min⁻¹ and 300,000 h⁻¹, respectively. The concentrations of NO, NO₂, N₂O and NH₃ were measured by Fourier Transform Infrared (FTIR) spectrometer (MKS-2030) equipped with a 5.11 m gas cell. Before this test, the catalyst was pretreated at 500 °C for 30 min by 5% O₂/N₂. SCR test condition was as following: 500 ppm NO, 500 ppm NH₃ and 5% O₂. Furthermore, the SCR tests in presence of 3% H₂O and 6% CO₂ over Cu-A and P10-F were also performed to prove their effect on NO conversion, and their concentrations were controlled at 3% and 6% in Fig. S1. The results agreed with our previous report about water and CO₂ influence on Cu/SAPO-34 catalysts that both of them did not inhibit NO conversion during test range. Therefore, we focus on standard SCR test without H₂O and CO₂ in this study to avoid their impact on ammonia adsorption and side-products generation [37]. The temperature was elevated from 120 °C to 600 °C, and the NO conversion was calculated as following Eq. (1):

$$\text{NO conversion}[\%] = \frac{\text{NO}_{\text{inlet}} - \text{NO}_{\text{outlet}}}{\text{NO}_{\text{inlet}}} \times 100[\%] \quad (1)$$

NH₃-SCR kinetic tests were performed in a thinner quartz tube using 25 mg catalyst and 125 mg quartz sand. The 80–100 mesh

particles sizes and 3,600,000 h⁻¹ volume hourly space velocity ensured the elimination of internal and external diffusion, respectively. Before the kinetic tests, catalysts were pretreated in 5% O₂/N₂ at 500 °C. The inlets contained 500 ppm NH₃, 500 ppm NO and 5% O₂ with N₂ as the balance. Kinetic steady-state measurements were conducted from 150 °C to 225 °C, and the reaction rates were calculated from NO_x conversion by Eq. (2):

$$\begin{aligned} \text{rate}[\text{mol NO}_x \cdot \text{g}_{\text{cata}} \cdot \text{s}^{-1}] \\ = \frac{X_{\text{NO}_x}[\%] \times F_{\text{NO}_x}[\text{L}(\text{NO}_x) \cdot \text{min}^{-1}]}{m_{\text{cata}} \times 60[\text{s} \cdot \text{min}^{-1}] \times 22.4[\text{L} \cdot \text{mol}^{-1}]} [\text{mol NO}_x \cdot \text{g}_{\text{cata}} \cdot \text{s}^{-1}] \quad (2) \\ X_{\text{NO}_x} = \text{NO}_x \text{ Conversion, } [\%]; \\ F_{\text{NO}_x} = \text{Flow Rate of NO}_x, [\text{L}(\text{NO}_x) \cdot \text{min}^{-1}] \end{aligned}$$

3. Results and discussion

3.1. Catalytic performance

3.1.1. Pt poisoning on fresh Cu/SAPO-34 samples

NH₃-SCR is firstly conducted to evaluate the performance variation caused by Pt presence. In addition, NH₃ oxidation and NO oxidation could further help us to analyze the SCR mechanism and side-products generation, and these three reactions are combined to conclude Pt poisoning to Cu/SAPO-34 catalysts.

3.1.1.1. NH₃-SCR results. Cu-F sample presents above 80% NO conversion from 200 °C to 430 °C in Fig. 1a, and its NO₂ and N₂O concentrations in Fig. 1b and c are less than 10 ppm, illustrating its excellent SCR activity and good N₂ selectivity during NH₃-SCR process. Compared with Cu-F sample, the presence of Pt increases the NO conversion under 250 °C and decreases NO conversion above 300 °C. The difference caused by Pt doping enlarges with the increment of its loading, meanwhile, Cu/P05-F and Cu/P10-F show the similar NO conversion. P10-F sample presents a narrow SCR activity window between 170 °C and 270 °C, and it loses SCR activity above 400 °C. In Fig. 1c, N₂O mainly appears around 250 °C over Pt doping samples and its concentration increases with the Pt loading. Similarly, NO₂ is generated above 250 °C and also increases with Pt loading in Fig. 1b. It is worth to mention that Cu/P10-F and P10-F contain the same Pt loading, but the former one shows higher NO conversion and lower side-products than later one, exposing the interaction between Cu sites and Pt sites on SCR reaction process. In addition, the N₂O and NO₂ generation are responsible for the NO conversion increase at low temperature and NO conversion

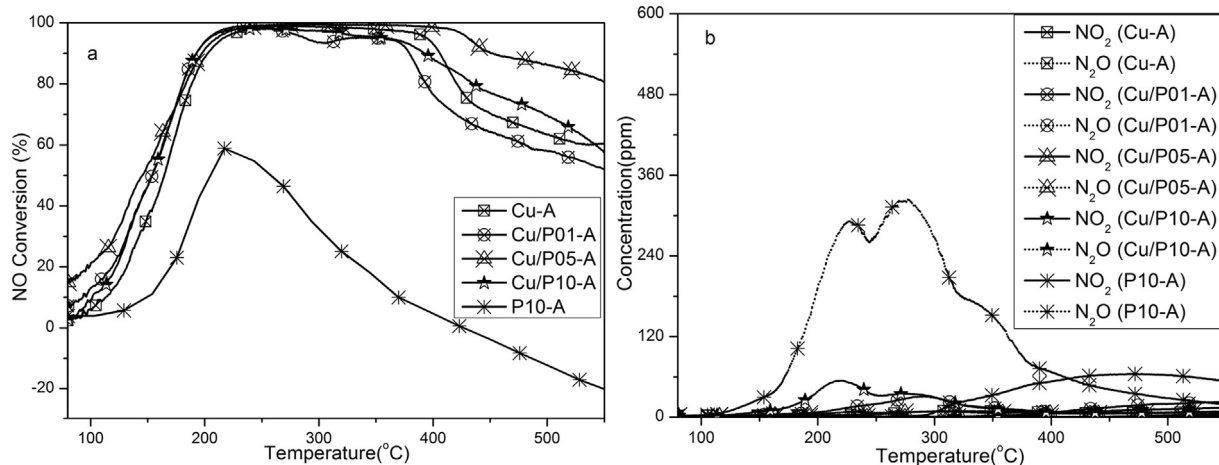


Fig. 4. NH₃-SCR performance of catalysts as a function of temperature. (a) NO conversion; (b) NO₂ and N₂O generation. The feed contained 500 ppm NH₃, 500 ppm NO, 5% O₂, N₂ was the balance. The flow rate and space velocity in all experiment were controlled at 500 mL min⁻¹ and 300,000 h⁻¹.

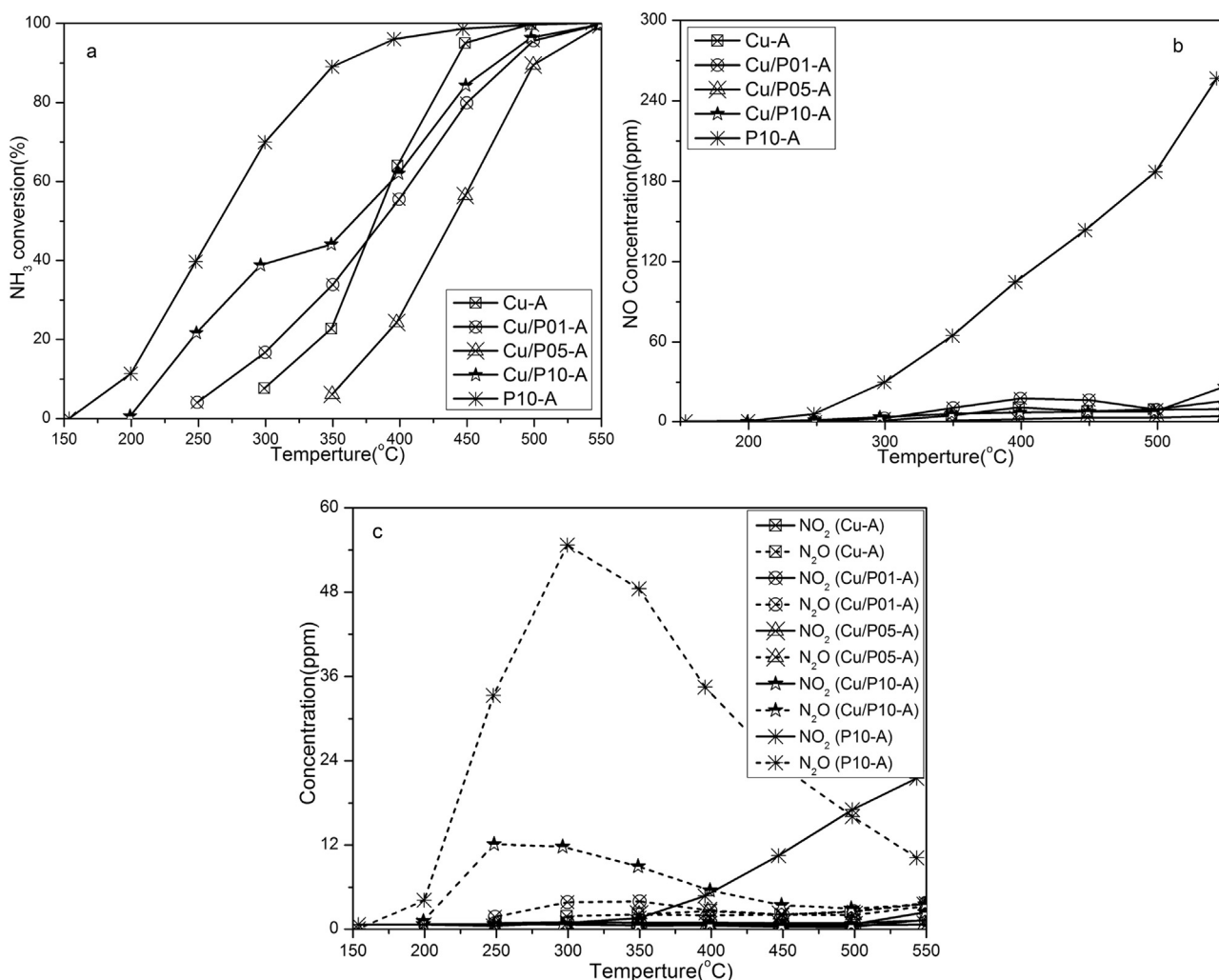


Fig. 5. NH₃ oxidation results over pure and Pt doping Cu/SAPO-34 catalysts. (a) NH₃ conversion; (b) NO concentration; (c) NO₂/N₂O concentration. The inlets consisted of 500 ppm NH₃, 5% O₂ with N₂ as the balance. The flow rate and volume hourly space velocity in all experiment were controlled at 500 mL min⁻¹ and 300,000 h⁻¹.

decrease at high temperature, which are also confirmed by nitrogen selectivity results in Fig. S19.

3.1.1.2. NH₃ oxidation results. Our previous study found the NO conversion at high temperature over Cu-F sample was mainly declined by NH₃ oxidation [22,36]. In Fig. 2a, NH₃ conversion keeps rising until 100% with the increment of temperature. Cu-F sample preforms the lowest NH₃ oxidation activity, and Pt doping improves NH₃ conversion during the whole temperature range. NO is the main products during NH₃ oxidation in Fig. 2b at high temperature and P10-F produces much more NO than others. In addition, N₂O and NO₂ also appear during this process. N₂O concentrations around 250 °C and NO₂ concentrations above 250 °C are enhanced due to the presence of Pt.

3.1.1.3. NO oxidation. In order to evaluate the reaction networks during NH₃-SCR process, NO oxidation over fresh samples is performed in Fig. 3. It is seen that Cu-F sample presents inferior NO conversion from 100 to 550 °C. For Pt-containing samples, the NO₂ desorption peaks around 150 °C are induced by nitrates decomposition and NO₂ desorption generated during pre-equilibrium process. Although Pt doping improves the NO conversion, NO conversions over all catalysts are less than 50%.

3.1.2. Regeneration of aged Cu/SAPO-34 samples after hydrothermal treatment

The above results reveal the contamination Pt decreases SCR activity of Cu/SAPO-34 sample. To evaluate the regeneration of poisoned Cu/SAPO-34 samples and characterize their hydrothermal stability, the fresh and Pt doping Cu/SAPO-34 samples are hydrothermally treated under 750 °C and their catalytic performance is showed as following.

3.1.2.1. NH₃-SCR results. After 750 °C treatment for 12 h, Cu-A maintains the excellent SCR activity during 120–550 °C, and its NO conversion is higher than that of Cu-F above 500 °C in Fig. 4a. The Cu/SAPO-34 sample was proved to exhibit good stability at 750 °C and hydrothermal treatment could improve its SCR activity due to the increase of Cu²⁺ contents [21]. Moreover, the aging treatment obviously improves the NO conversion of Pt doping Cu/SAPO-34 samples. During high temperature range, Cu/P01-A presents 10% lower NO conversion than Cu-A sample, while Cu/P05-A and Cu/P10-A even show higher NO conversions than Cu-A. However, P10-A shows lower NO conversion than P10-F under 400 °C, and it generates less NO at high temperature after aging treatment. The decline of SCR activity over P10-A illustrates the Pt sintering during hydrothermal treatment.

Fig. 4b shows the N₂O and NO₂ generation during NH₃-SCR process. Compared with fresh samples, the aging treatment greatly

Table 2
Products of gas switching tests.

Sample	230 °C			430 °C		
	NO + O ₂	NH ₃ + O ₂	NO + NH ₃	NO + O ₂	NH ₃ + O ₂	NO + NH ₃
Cu-F	/	/	Less N ₂ O	Less NO ₂	NO	N ₂ O
Cu/P05-F	/	N ₂ O	Less N ₂ O	NO ₂	N ₂ O, NO, NO ₂	N ₂ O
P10-F	Less NO ₂	N ₂ O	N ₂ O	NO ₂	N ₂ O, NO, NO ₂	Less NO ₂

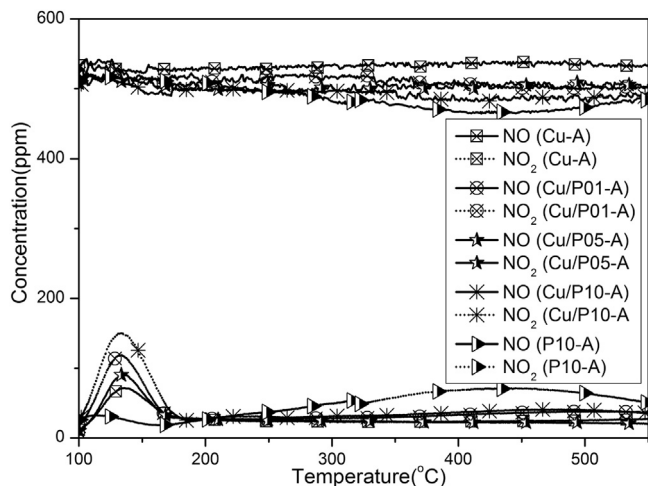


Fig. 6. NO oxidation results over aged Cu/SAPO-34 catalysts. The inlets consisted of 500 ppm NO, 5% O₂ with N₂ as the balance. The flow rate and volume hourly space velocity in all experiment were controlled at 500 mL·min⁻¹ and 300,000 h⁻¹.

declines side products concentrations, which is also proved by the high nitrogen selectivity results in Fig. S19. N₂O is less than 60 ppm for Pt doping Cu/SAPO-34 samples and NO₂ is less than 20 ppm above 400 °C. P10-A produces the most side products than others, but their concentrations become half of that over P10-F in Fig. 1b.

It is seen that the hydrothermal treatment at 750 °C could partially recover the SCR activity of Pt doping Cu/SAPO-34 samples, so it is wondered whether a higher treatment temperature without structure collapse and over Pt doping Cu/SAPO-34 completely regain their NO conversions. Considering the hydrothermal treatment above 850 °C could damage the SAPO-34 structure, Cu/P10-F and P10-F are chosen to be hydrothermally treated at 850 °C for 6 h to evaluate its regeneration due to their highest Pt contents for convenient detection. [22] In Fig. S1 (Supplementary information), 850 °C treatment greatly improves SCR activity of Cu/P10-A-850, and its NO conversion is even higher than Cu-F in Fig. 1a. Moreover, the N₂O and NO₂ concentrations sharply decrease over Cu/P10-A-850 sample. It is concluded that the hydrothermal treatment could inhibit Pt poisoning on Cu/SAPO-34 sample and benefit their rejuvenation if the temperature is not high enough to destroy its framework.

In Fig. S2a, P10-A-850 sample presents the similar NO conversion as P10-A, and both of them show the lower NO conversion than P10-F under 300 °C. The higher NO conversion over fresh sample may be due to its higher Pt dispersion. In addition, the higher NO conversion at low temperature causes the increase of side-products in Fig. S2b.

3.1.2.2. NH₃ oxidation results. NH₃ oxidation results over aged samples are showed in Fig. 5. Except P10-A sample, all Pt doping samples reveal the similar NH₃ conversion with Cu-A sample. P10-A still presents the highest NH₃ conversion during the whole temperature, illustrating its strong ammonia oxidation ability. Nevertheless, the NH₃ conversions over Pt doping aged Cu/SAPO-34 samples decrease compared with the fresh ones in Fig. 2a. Fur-

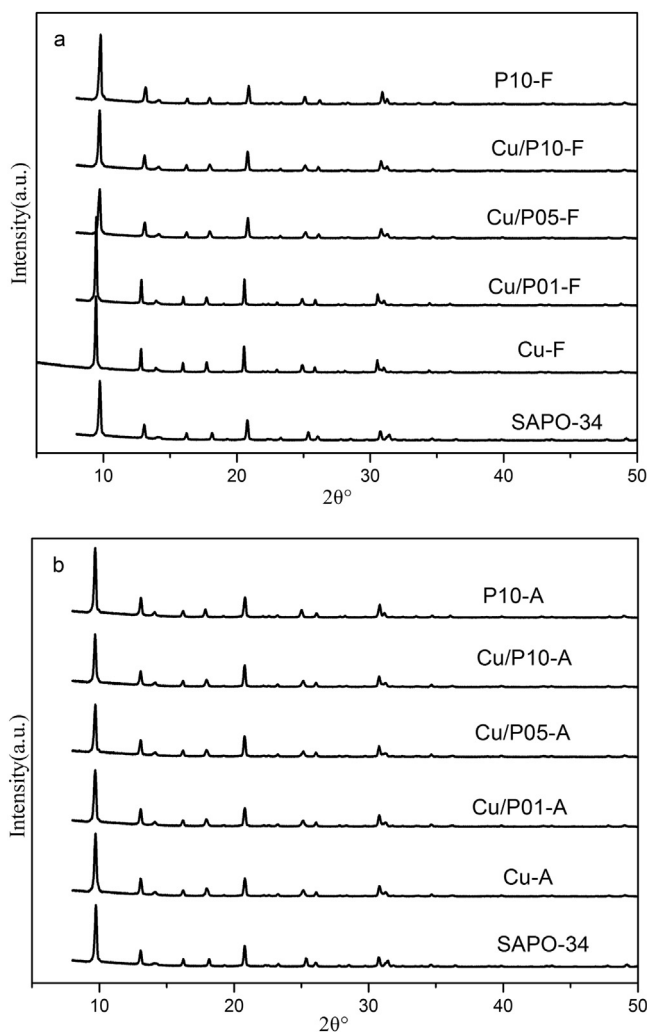


Fig. 7. XRD profiles of all (a) fresh and (b) aged molecular sieves.

thermore, the NO generation greatly declines in Fig. 5b, and its concentration is less than 30 ppm during this process except P10-A. The NO₂ and N₂O concentrations simultaneously decrease after hydrothermal treatment.

In addition, NH₃ oxidation over Cu/P10-A-850 sample was also conducted to evaluate regeneration of Pt poisoned Cu/SAPO-34 sample. Fig. S3a reveals the hydrothermal treatment weakens NH₃ oxidation activity, which benefits the increase of NO conversion at high temperature. Fig. S3b and S3c both expose the decrease of side-products over aged samples. The treatment at 750 °C and 850 °C presents the same weakening trend on NH₃ oxidation over Cu/P10 samples.

The hydrothermal treatment also decreases NH₃ oxidation activity and side-products generation over P10-A-850 in Fig. S4. This phenomenon is mainly related to the Pt sintering, which will be explained later in detail.

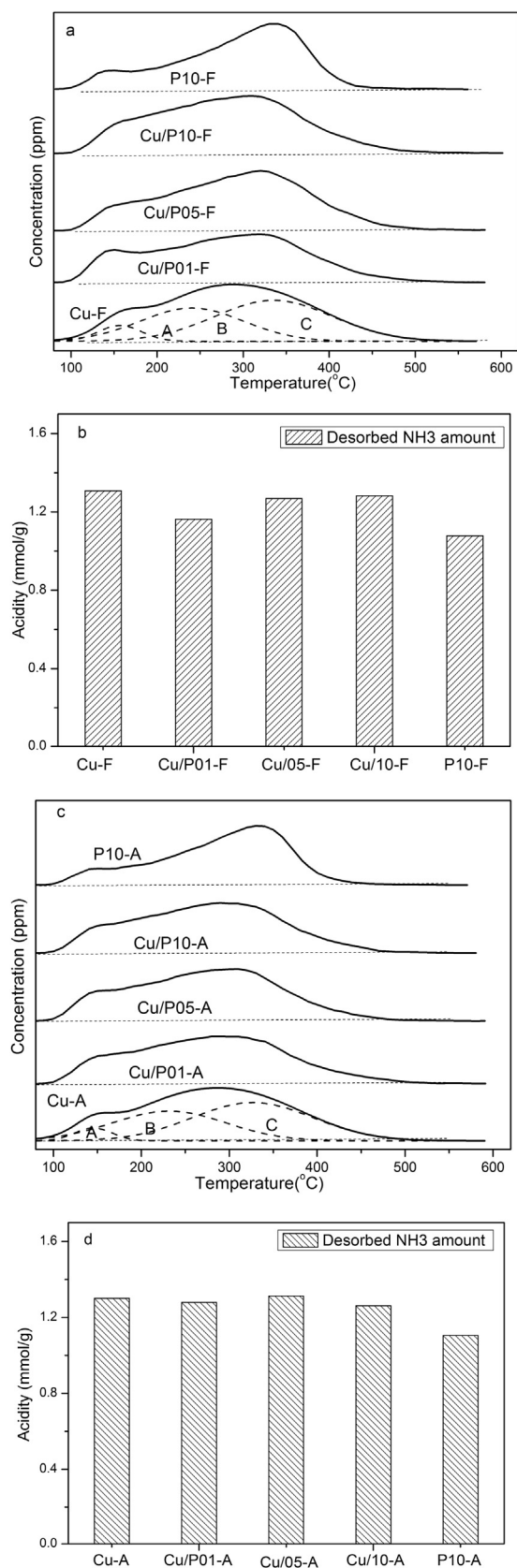


Fig. 8. NH_3 -TPD results of (a) fresh and (c) aged samples, and the integrated ammonia desorption amounts over (b) fresh and (d) aged samples. NH_3 -TPD experiment was ramped from 80 °C to 600 °C at a rate of 10 °C/min.

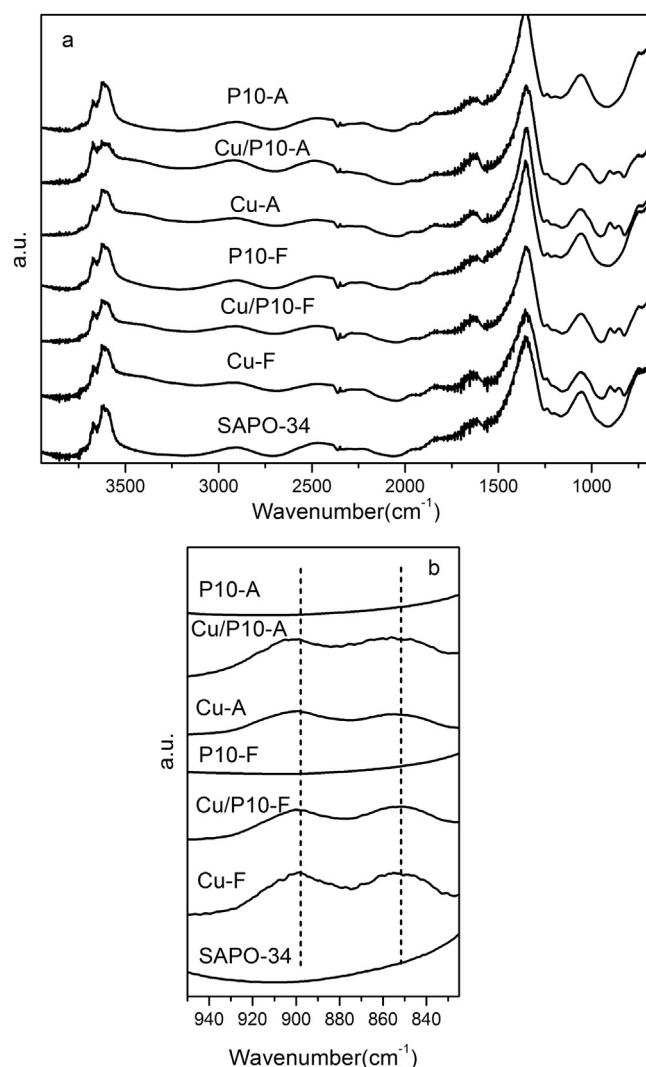


Fig. 9. Ex-situ DRIFTS of all samples. (a) Range between 680 and 4200 cm^{-1} ; (b) Range between 780 and 1000 cm^{-1} .

3.1.2.3. NO oxidation. In Fig. 6, all aged samples perform inferior NO oxidation and P10-A shows the highest NO conversion over 300 °C. Compared with fresh Cu/SAPO-34 samples in Fig. 3, all aged samples present lower NO oxidation activity, while the aged ones perform better SCR activity than fresh ones, which illustrates NO oxidation is not the dominant factor to SCR activity over Cu/SAPO-34 samples.

In addition, the influence of hydrothermal temperature on NO oxidation over Cu/P10 and P10 samples is showed in Fig. S5 and S6. It is seen that the high temperature treatment clearly decreases the NO conversion, and 750 °C and 850 °C treatments show the similar effect on them.

3.1.3. Gas switching tests

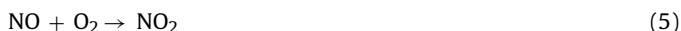
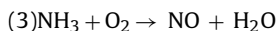
To completely understand the Pt influence on side-products generation and N_2 selectivity decrease, three samples (Cu-F, Cu/P05-F and P10-F) are utilized to conduct reactants switching tests, including: NO oxidation ($\text{NO} + \text{O}_2$), ammonia oxidation ($\text{NH}_3 + \text{O}_2$) and oxygen free SCR ($\text{NO} + \text{NH}_3$). The tests are performed at low and high temperature and concluded in Table 2, respectively.

3.1.3.1. Cu-F. At 230 °C in Table 2/ Fig. S7, there is no NO oxidation and NH_3 oxidation detected over Cu/SAPO-34 sample. The 25 ppm NO_2 in NO oxidation comes from the NO cylinder source and less

N₂O is detected. NH₃ + NO only generate less N₂O, which all reveals its excellent N₂ selectivity.

For the tests at 430 °C in Table 2/ Fig. S8, less NO₂ is produced from NO oxidation. In addition, only 8 ppm NO is detected during NH₃ oxidation as Eq. (3), and this causes NO conversion decline at high temperature due to ammonia consumption competition. NH₃ + NO generate 12 ppm N₂O over Cu/SAPO-34 sample as Eq. (4) at high temperature.

3.1.3.2. Cu/P05-F. For 230 °C in Table 2/ Fig. S9, it is seen that almost no NO oxidation happens over Cu/P05-F sample. For NH₃ oxidation, 9 ppm N₂O is generated as Eq. (6). In addition, NO + NH₃ reaction produces less N₂O as Eq. (4).



For 430 °C in Table 2/ Fig. S10, it is clear that 115 ppm NO₂ generates from NO oxidation as Eq. (5). And NH₃ oxidation generates 9 ppm N₂O, 47 ppm NO and 23 ppm NO₂ at 430 °C as Eqs. (3), (6) and (7). In addition, 32 ppm N₂O is detected during NO + NH₃ as Eq. (4).



3.1.3.3. P10-F. For P10-F at 230 °C in Table 2/ Fig. S11, less NO₂ is produced from NO oxidation. But the NH₃ oxidation generates 90 ppm N₂O as Eq. (6), and Pt presence enhances this NH₃ oxidation compared with Cu/P05-F sample. In addition, NO + NH₃ generate 60 ppm N₂O without oxygen over Pt sites as Eq. (4).

At 430 °C in Table 2/ Fig. S12, 195 ppm NO₂ is generated from NO oxidation as Eq. (5). NH₃ oxidation also produces 170 ppm NO, 100 ppm NO₂ and 18 ppm N₂O simultaneously. However, NH₃ + NO could not generate N₂O and less NO₂ is detected.

Overall, Cu/SAPO-34 presents excellent N₂ selectivity during the whole temperature, while the presence of Pt greatly enhances N₂O and NO₂ formation, accounting for massive byproducts in Fig. 1. At low temperature, Pt loading increment enhances N₂O generation from ammonia oxidation by oxygen and NO due to its higher oxidation ability, which reflects Pt species does not affect essential SCR reaction mechanism of Cu/SAPO-34 sample. At high temperature, N₂O is mainly generated by NH₃ oxidation, and NO₂ comes from NO oxidation in presence of Pt.

3.2. Sample characterization

3.2.1. XRD results

The XRD profiles show Cu and Pt loading do not affect CHA structure in Fig. 7a, and 750 °C hydrothermal treatment also shows less influence on SAPO-34 structure in Fig. 7b [35]. In addition, there are no copper oxides or Pt species peaks detected, which illustrates their well dispersion over SAPO-34 molecular sieve or smaller sizes under detection limitation. And excellent structure stability ensures the following discussion without skeleton collapse.

3.2.2. NH₃-TPD results

In order to examine Pt impact on frameworks hydroxyls and SAPO-34 acidity, NH₃-TPD is performed in Fig. 8. Fig. 8a shows three NH₃ desorption peaks over all samples, and these detailed ascription have been showed in previous works [21,26]. For fresh Cu/SAPO-34 sample, the low temperature peak (A) represents NH₃ molecules adsorbed on weak Lewis acid sites related to Cu species

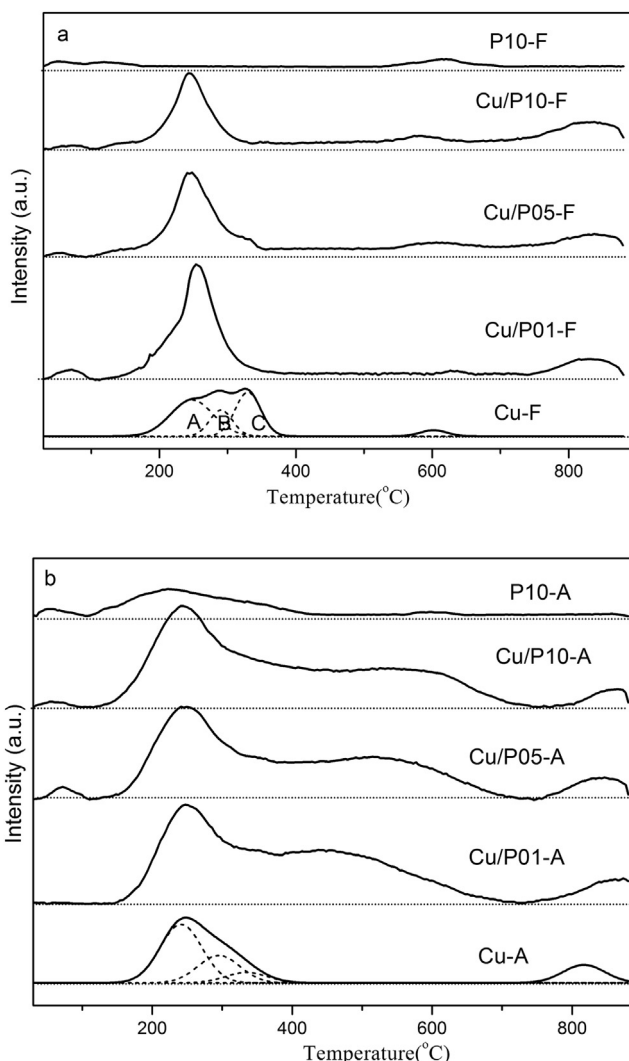


Fig. 10. H₂-TPR results of all catalysts. The feed contained 5 vol% H₂/N₂ and fed at a flow rate of 15 mL min⁻¹. The experiment was performed from 30 °C to 900 °C with the heatingup rate of 5 °C/min.

and weak Brønsted acid sites (surface hydroxyl). The two peaks at higher temperature (B and C) present the NH₃ species adsorbed on strong acid sites of structural Brønsted acid sites (Si—OH—Al) and new Lewis acid sites created by Cu²⁺ species. For Pt doping samples, Pt presence shows less influence on their acidity through its comparison with support in supplementary information, illustrating no Brønsted acid sites replacement by Pt species. P10-F sample almost performs the same NH₃ desorption peaks with SAPO-34 support, proving its no incorporation with skeleton hydroxyls and less influence on acidity. After 750 °C hydrothermal treatment, Fig. 8c shows the similar ammonia desorption results with fresh samples and no obvious variation on acidity of Cu/SAPO-34 samples.

3.2.3. Ex-situ DRIFTS

To further confirm the Cu and Pt location over SAPO-34 molecular sieve, *ex-situ* DRIFTS are performed in Fig. 9, and two framework vibrations regions reveal variation related hydroxyls substitution in skeleton. Firstly, the peaks at 3625 and 3600 cm⁻¹ are related to the —OH group stretching vibration modes (Al—OH—Si) [35]. In addition, two bands at 891 and 845 cm⁻¹ are associated with an internal asymmetric framework vibration perturbed by Cu²⁺ species [21]. Compared with SAPO-34 support, fresh Cu/SAPO-34 sample shows lower OH group stretching vibration peaks around 3600 cm⁻¹ and

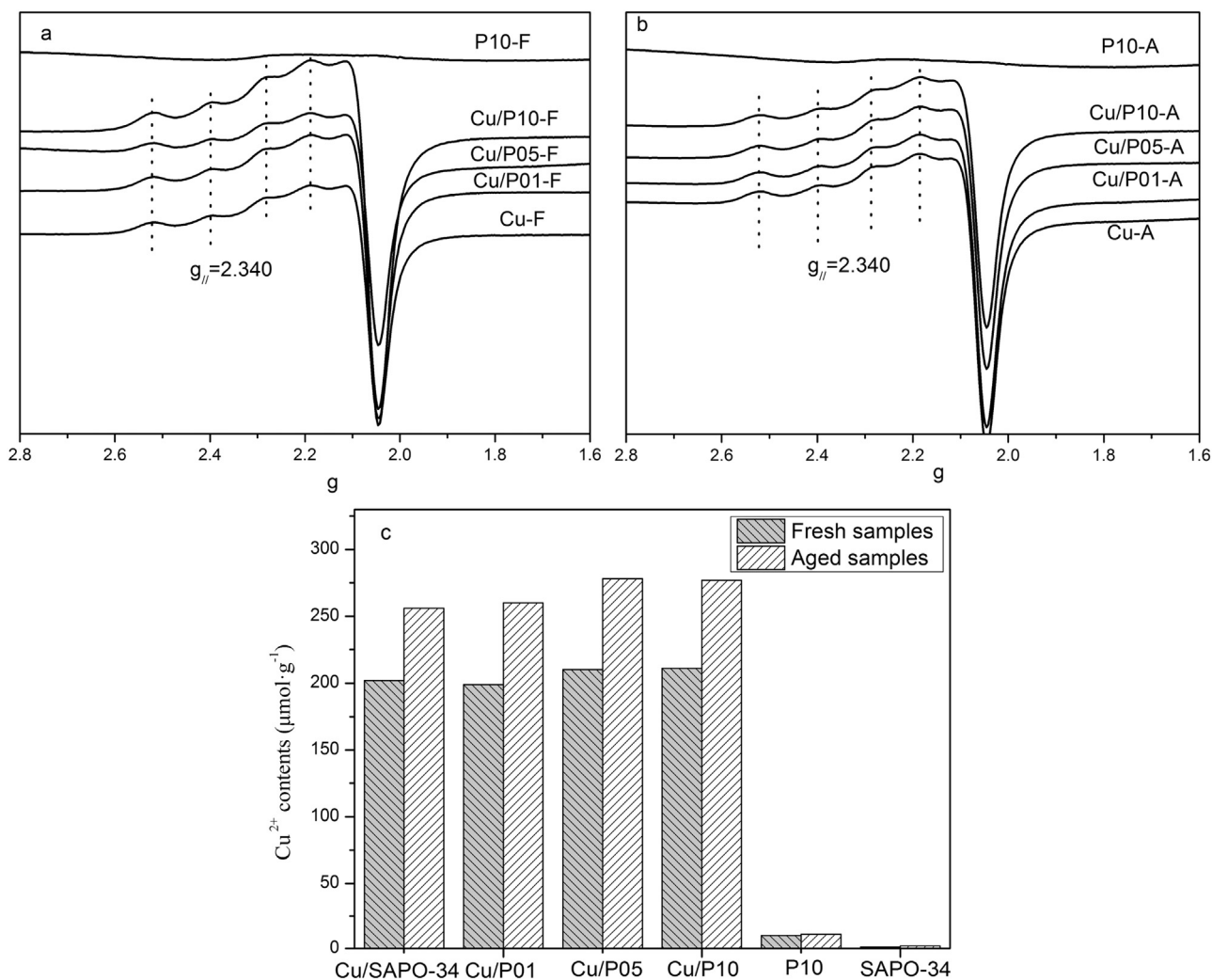


Fig. 11. EPR results of all catalysts. The samples were pretreated at 120 °C for 48 h.

two new peaks at 891 and 845 cm⁻¹, which are mainly induced by isolated Cu²⁺ through hydroxyls replacement. Nevertheless, Pt doping almost has no influence on SAPO-34 frameworks over P10-F sample. After 750 °C hydrothermal treatment, aged Cu/SAPO-34 samples still maintain the same structure and still no interaction between Pt and framework is detected. It is concluded that doped Pt species do not incorporate with SAPO-34 skeleton as isolated Cu²⁺ species through hydroxyl substitution.

3.2.4. H₂-TPR results

As we studies before, Cu/SAPO-34 sample contains CuO, Cu⁺ species and Cu²⁺ species [21,22]. For fresh Cu/SAPO-34 sample, Fig. 10a shows three main reduction peaks during 200 °C and 400 °C: peak A is induced by isolated Cu²⁺ reduction to Cu⁺; the peak C at the high temperature is induced by Cu⁺ reduction to Cu⁰, and the peak B represents the bulk copper oxide reduction in zeolites from CuO to Cu⁰. In addition, H₂ consumption peaks higher than 500 °C are ascribed to highly stable Cu⁺ reduction to Cu⁰ [21]. For P10-F sample, Pt mainly keeps reduced Pt⁰ state due to no peak from its TPR profile. For Pt poisoned Cu/SAPO-34 samples, the CuO and Cu⁺ peaks all shift to lower temperature and this influence becomes more obvious with the increment of Pt contents. For Cu/P05-F and Cu/P10-F samples, there is almost only one symmetric reduction peak, which means Pt species enhance Cu²⁺ species reduction from Cu²⁺ to Cu⁰. In addition, CuO reduction peaks shift

to lower temperature and overlap with Cu²⁺ reduction, and we predict the doped Pt species tend to bond with CuO species, presenting hydrogen spillover impact on copper sites and benefiting their reduction and improving their redox potential.

After 750 °C hydrothermal treatment, aged Cu/SAPO-34 sample also presents Cu²⁺ species, CuO and Cu⁺ species reduction peaks, but CuO content decreases due to promotion of this treatment on CuO re-dispersion to isolated Cu²⁺ species in Fig. 10b [21]. For P10-A sample, a wide peak around 200 °C is Pt oxides reduction. For Pt poisoned samples, Cu²⁺ species present increasing trend compared with Cu-A sample, illustrating the positive influence of Pt species on CuO re-dispersion. And this hemi-quantification will be further conducted in the following EPR study. Furthermore, new wide peak appears around 500 °C and it is ascribed to the reduction Pt-Cu oxides complex, which will be illustrated in following STEM results. In addition, this peak shifts to higher temperature with platinum contents increase related to their composition. The increase Pt loading can decrease the valence of Cu species to Cu⁺ and increase their reduction temperature. Compared with metallic platinum states in fresh samples, platinum species show oxidized states after hydrothermal treatment. During 750 °C hydrothermal treatment, the reduced Pt could seize the oxygen atoms form CuO species and enhance their transformation to Cu²⁺ species which will be discussed later.

In addition, the aging temperature impact on copper species reduction is showed in Fig. S13 over Cu/P10 series samples, illustrating the interaction between Cu and Pt species. For fresh Cu/P10-F sample, Pt keeps reduced state and greatly accelerates CuO species reduction by hydrogen, revealing the interaction between CuO and Pt species. After 750 °C hydrothermal treatment, Pt species interact with CuO species and form oxide complexes, performing wide reduction peak 500 °C. Moreover, these Pt-Cu oxo-complexes present lower reduction temperature over Cu/P10-850 than Cu/P10-A, which is induced by oxides sintering. Therefore, it is predicted that Pt species mostly locates alone with CuO species and are oxidized after hydrothermal treatment.

In addition, XPS profiles in Fig. S15 further unveil the copper and platinum states and behavior during aging treatment. For all tested samples, the binding energy of 934.2 eV for the Cu 2p_{3/2} peak of Cu²⁺ species is detected [23,38,39], while only fresh samples present CuO species signal around 955 eV, which implies the further copper distribution during aging treatment. For fresh Pt containing samples, Pt signals appear around 71.6 eV and is in the elemental form with Pt 4f_{7/2} BE electrons. But after aging treatment even highest Pt doping samples preform no metallic Pt related signals, which may be induced by their sintering [40,41].

3.2.5. EPR results

EPR is only sensitive to isolated Cu²⁺ species but not active to CuO and Cu⁺ in Cu/SAPO-34, which can be used to examine the Cu²⁺ coordination variation and Pt influence during aging treatment in Fig. 11 [21]. For the fresh samples, they present hyperfine structure of Cu²⁺ species with typical four peaks in EPR profile ($g_{||} = 2.340$), while P10-F presents no EPR signal. For the three Pt poisoned samples, they present the same Cu²⁺ hyperfine structure, illustrating no influence of Pt on Cu²⁺ electrical coordination in skeleton. Cu²⁺ species quantification, through CuSO₄ EPR working curve as our previous report, is listed in Fig. 11c, and the Cu²⁺ contents almost keep similar constant [35].

After hydrothermal treatment at 750 °C, the aged samples show the same Cu²⁺ species hyperfine peaks with fresh ones, but Cu²⁺ contents increase. It is known that hydrothermal treatment could accelerate CuO further distribution into isolated Cu²⁺ species, and this caused NO conversion increase during NH₃-SCR process over aged Cu/SAPO-34 samples [21]. Moreover, compared with aged Cu/SAPO-34 sample, the Cu²⁺ contents seem to be further improved with Pt presence, which indicates the Pt could enhance the distribution of CuO. Our previous study showed that this further distribution followed the route of CuO → Cu → Cu²⁺, and the Pt might enhance the decomposition of CuO and benefit Cu²⁺ increase [23]. In addition, Cu-F, Cu-A and Cu-A-850 quantification results in Fig. S14 reveal the aging treatment enhances copper species further distribution under the premise of less structure collapse.

3.3. Pt poisoning effect on Cu/SAPO-34 catalyst

Pt poisoning impact on NH₃-SCR mainly exhibits the N₂O generation at low temperature range and NH₃ oxidation increase at high temperature in Figs. 1 and 2. In order to evaluate the SCR mechanism variation, the kinetic tests are performed at low temperature. Fig. 12a presents apparent activation energy (E_a) for NH₃-SCR over fresh samples, and they follow the sequence as: P10-F (20.8 kJ/mol) < Cu/P10-F < Cu/P05-F < Cu/P01-F < Cu/SAPO-34 (58.9 kJ/mol). Compared with Cu/SAPO-34 sample, the decreasing E_a trend indicates the SCR mechanism variation, which causes NO conversion increase over Pt-containing samples in Fig. 1 at low temperature. For P10-F sample, it performs different NH₃-SCR pathway and the products are mainly N₂O at low temperature. But for Cu/SAPO-34 sample, the SCR products are mainly N₂. P10-F performs higher NO conversion due to its lower apparent E_a than later

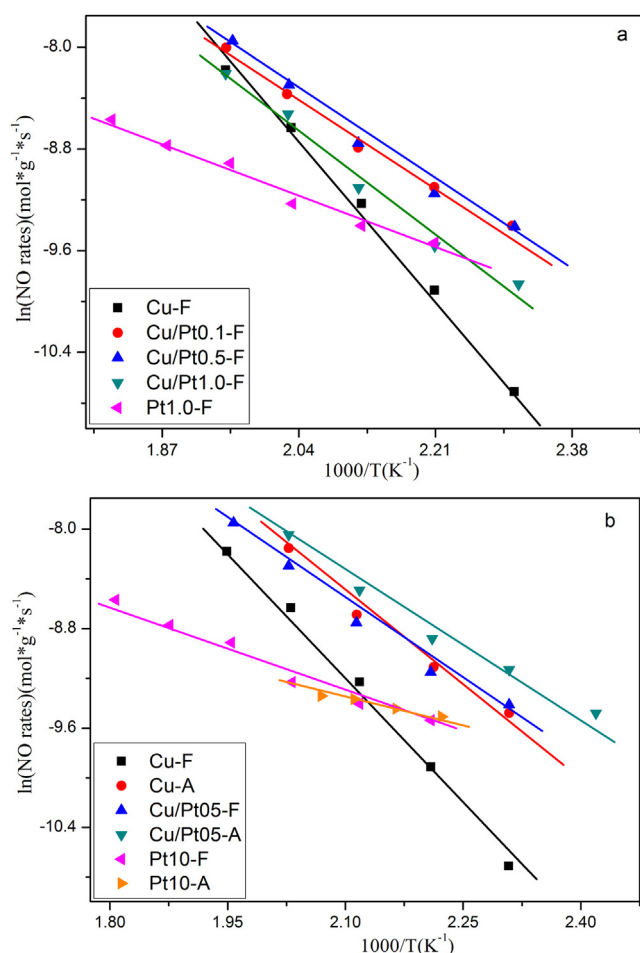


Fig. 12. NH₃-SCR kinetic results of all catalysts at low temperature. The feed contained 500 ppm NO, 500 ppm NH₃, 5% O₂ and N₂ as balance. The flow rate was 12,000 mL/min.

one. Consequently, with the increase of Pt contents in Cu/SAPO-34 samples, apparent E_a decrease and NO conversions increase, and N₂O generation increase at low temperature consequently. The varied SCR performance in Fig. 1a is induced by Pt species in Cu/SAPO-34 samples. The TPR results in Fig. 10a confirm reducing state of Pt species in fresh samples and they also performed NH₃-SCR activity in previous studies [42]. And the decreased E_a are caused by both different NO conversions reactions over two active sites of Cu²⁺ and Pt sites.

For fresh samples at high temperature, Pt poisoning mainly exhibits NH₃ oxidation increase in Fig. 2 and the main product is NO, both of which cause NO conversion decrease at high temperature. Pt species in Cu/SAPO-34 samples present strong oxidation ability and strengthen ammonia oxidation competition with NH₃-SCR. The TPR results in Fig. 10a reveal the metallic Pt⁰ species, which is another ammonia oxidation active site from Table 2 and responsible for the superior ammonia oxidation activity. In addition, *ex-situ* DRIFTS and NH₃-TPD confirm Pt does not incorporate with hydroxyls as Cu²⁺ species, therefore, we utilize STEM in Fig. S16 to examine that Pt⁰ particles mainly exist on the outside surface of SAPO-34 particles. The images present 1–10 nm Pt⁰ species on fresh Cu/SAPO-34 surfaces clearly.

3.4. Regeneration of Pt modified Cu/SAPO-34 after hydrothermal treatment

In Fig. 4, NH₃-SCR activity over Pt poisoned samples mostly recovers after hydrothermal treatment and the side-products generation decreases as Cu/SAPO-34 sample. Firstly, this is mainly

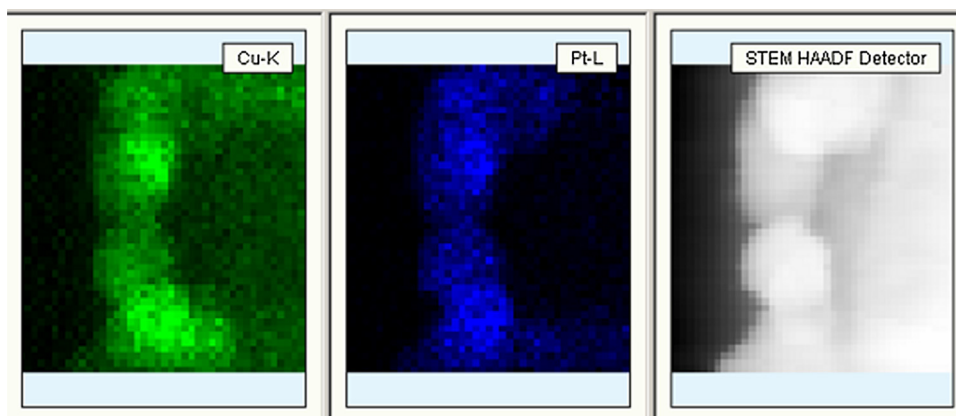


Fig. 13. STEM images of Cu, Pt mapping over aged Cu/PtO_x-A sample.

induced by Pt sintering and platinum oxides formation on zeolites. The TPR results in Fig. 10b have showed PtO reduction peak in P10-A sample, which also exists in other Pt containing samples after hydrothermal treatment. And the STEM images in Fig. S16 clearly illustrate the sintering Pt oxides particles (20–100 nm) on the surface, much bigger than corresponding fresh ones. And P10-A sample in Figs. 4 and 5 performs lower NO conversion and ammonia conversion than P10-F sample, illustrating inferior SCR activity and ammonia oxidation activity of platinum oxides and decrease of metallic Pt species. Meanwhile, compared with P10-A sample, other Pt poisoned Cu/SAPO-34 samples could regenerate and the side-products production mostly declines compared with the corresponding fresh samples. This is also caused by the Cu²⁺ contents increase and copper-platinum oxo-complexes formation. EPR results in Fig. 11 expose the calculated Cu²⁺ contents and the aged ones contain more active sites than the fresh ones due to further copper oxide distribution during hydrothermal treatment. And it is intriguing that Cu²⁺ increase contents in Pt containing samples are higher than that over aged Cu/SAPO-34 sample. It is already proved that CuO species could further transform into Cu²⁺ species by hydrothermal treatment, furthermore, Pt presence could enhance copper oxide disassociation and then Cu²⁺ transformation process as discussed in EPR results. Moreover, the H₂-TPR results show there is a wide peak around 500 °C and this is ascribed into the copper-platinum oxide complexes, which weakens ammonia oxidation over copper oxides sites. In order to confirm their existence, STEM and area scanning are performed to examine dispersion and interaction between copper oxides and Pt oxide species. Then the STEM elemental mapping over a random particle is conducted in Fig. 13 and the image presents it is composed by copper and platinum oxides. It is known that CuO inhibits NO conversion due to their oxidation ability of ammonia at high temperature, but the formation of this copper-platinum oxide complexes poison its oxidizing ability actually, benefiting SCR activity at high temperature [36]. Overall, after hydrothermal treatment at 750 °C, Cu²⁺ contents increase in aged samples, meanwhile, copper-platinum oxide complexes simultaneously generate and limit the side reaction induced by copper and platinum oxides. Therefore, Pt poisoned Cu/SAPO-34 samples could regenerate after hydrothermal treatment, and their SCR activities even higher with treatment temperature increase on conditions that the temperature does not damage its structure. The similar Ea values comparison between fresh and aged samples in Fig. 12b also indicates less Pt impact on SCR reaction mechanism over Cu/SAPO-34 catalysts.

4. Conclusion

This study mainly exposes platinum inhibition on NH₃-SCR activity and its interaction with copper species in zeolites, and then

confirms the rejuvenation of Cu/SAPO-34 after hydrothermal stability and the intrinsic mechanism. Firstly, platinum mainly exists as metallic states in Cu/SAPO-34 outside surface and does not incorporate with hydroxyls as Cu²⁺ species. It presents less influence on zeolites structure and acidity, but greatly poisons NH₃-SCR activity. Pt presence increases NO conversion at low temperature but greatly increase N₂O formation. This is induced by different SCR pathway over platinum sites and decreases nitrogen selectivity. Moreover, Pt presence benefits ammonia oxidation at high temperature, which greatly inhibits NO conversion over Cu/SAPO-34 through ammonia competition consumption. In addition, hydrothermal treatment benefits rejuvenation of Pt poisoned Cu/SAPO-34 catalysts, and 850 °C treatment even leads to higher NO conversion than aged Cu/SAPO-34. Hydrothermal treatment causes Pt sintering and platinum oxides formation, and also enhances copper oxides transformation into Cu²⁺ species and copper-platinum oxo-complexes. Pt sintering and oxides formation weakens their ammonia oxidation ability and SCR poisoning, meanwhile, the increase of active sites further increase NO conversions. The copper-platinum oxo-complexes is a new starting point to understand copper oxides deactivation on ammonia oxidation and improve SCR activity at high temperature.

Acknowledgement

The authors would like to acknowledge GM Global Research & Development (RD-11-368 GB945-NV-HY) for the financial support of this project. This work was also supported by the National Natural Science Foundation of China (21676195). Meanwhile, the author thanks the support from China Scholarship Council (CSC) and excellent post-doctorate scholarship from Dalian Institute of Chemical Physics, CAS.

Appendix A. Supplementary data

Supplementary data associated with this article can be found, in the online version, at <http://dx.doi.org/10.1016/j.apcatb.2016.12.007>.

References

- [1] Z. Liu, J. Li, S.I. Woo, *Energy Environ. Sci.* 5 (2012) 8799–8814.
- [2] P. Forzatti, *Appl. Catal. A-Gen.* 222 (2001) 221–236.
- [3] J. Li, H. Chang, L. Ma, J. Hao, R.T. Yang, *Catal. Today* 175 (2011) 147–156.
- [4] T.V. Johnson, *Int. J. Engine Res.* 10 (2009) 275–285.
- [5] Selective catalytic reduction of nitrogen oxides by ammonia, in: S.W. Ham, I.S. Nam, J.J. Spivey (Eds.), *Catalysis*, vol. 16, The Royal Society of Chemistry, Cambridge, 2002, pp. 236–271.
- [6] K.I. Shimizu, A. Satsuma, *Phys. Chem. Chem. Phys.* 8 (2006) 2677–2695.
- [7] L.J. Alemany, L. Lietti, N. Ferlazzo, P. Forzatti, G. Busca, E. Giamello, F. Bregani, *J. Catal.* 155 (1995) 117–130.

- [8] Z. Ma, D. Weng, X. Wu, Z. Si, B. Wang, *Catal. Commun.* 27 (2012) 97–100.
- [9] R.Q. Long, R.T. Yang, *Appl. Catal. B: Environ.* 24 (2000) 13–21.
- [10] M. Kobayashi, R. Kuma, S. Masaki, N. Sugishima, *Appl. Catal. B: Environ.* 60 (2005) 173–179.
- [11] A. Uddin, T. Komatsu, T. Yashima, *J. Chem. Soc. Dalton Trans.* 91 (1995) 3275–3279.
- [12] A. Schuler, M. Votsmeier, P. Kiwic, J. Gieshoff, W. Hautpmann, A. Drochner, H. Vogel, *Chem. Eng. J.* 154 (2009) 333–340.
- [13] Y.J. Kim, J.K. Lee, K.M. Min, S.B. Hong, I.-S. Nam, B.K. Cho, *J. Catal.* 311 (2014) 447–457.
- [14] U. Deka, A. Juhin, E.A. Eilertsen, H. Emerich, M.A. Green, S.T. Korhonen, B.M. Weckhuysen, A.M. Beale, *J. Phys. Chem. C* 116 (2012) 4809–4818.
- [15] A.Z. Ma, W. Grunert, *Chem. Commun.* 1 (1999) 71–72.
- [16] D.W. Fickel, E. D'Addio, J.A. Lauterbach, R.F. Lobo, *Appl. Catal. B: Environ.* 102 (2011) 441–448.
- [17] J.H. Kwak, R.G. Tonkyn, D.H. Kim, J. Szanyi, C.H.F. Peden, *J. Catal.* 275 (2010) 187–190.
- [18] T. Tanabe, T. Iijima, A. Koiwai, J. Mizuno, K. Yokota, A. Isogai, *Appl. Catal. B: Environ.* 6 (1995) 145–153.
- [19] I. Bull, W.-M. Xue, P. Burk, R.S. Boorse, W.M. Jaglowski, G.S. Koerner, A. Moini, J.A. Patchett, J.C. Dettling, M.T. Caudle, U.S. Patent, 7610662, 2009.
- [20] P.J. Andersen, J.E. Bailie, J.L. Casci, H.-Y. Chen, J.M. Fedeyko, R.K.S. Foo, R.R. Rajaram, U.S. Patent, 2010/0290963, 2010.
- [21] J. Wang, T. Yu, X. Wang, G. Qi, J. Xue, M. Shen, W. Li, *Appl. Catal. B: Environ.* 127 (2012) 137–147.
- [22] J. Wang, Y. Huang, T. Yu, S. Zhu, M. Shen, W. Li, J. Wang, *Catal. Sci. Technol.* 4 (2014) 3004–3012.
- [23] L. Wang, J.R. Gaudet, W. Li, D. Weng, *J. Catal.* 306 (2013) 68–77.
- [24] L. Wang, W. Li, G. Qi, D. Weng, *J. Catal.* 289 (2012) 21–29.
- [25] H. Zhu, J.H. Kwak, C.H.F. Peden, J. Szanyi, *Catal. Today* 205 (2013) 16–23.
- [26] T. Yu, J. Wang, M. Shen, W. Li, *Catal. Sci. Technol.* 3 (2013) 3234–3241.
- [27] L. Ma, Y. Cheng, G. Cavataio, R.W. McCabe, L. Fu, J. Li, *Appl. Catal. B: Environ.* 156/157 (2014) 428–437.
- [28] I. Lezcano-Gonzalez, U. Deka, B. Arstad, A. Van Yperen-De Deyne, K. Hemelsoet, M. Waroquier, V. Van Speybroeck, B.M. Weckhuysen, A.M. Beale, *Phys. Chem. Chem. Phys.* 16 (2014) 1639–1650.
- [29] S. Fan, J. Xue, T. Yu, D. Fan, T. Hao, M. Shen, W. Li, *Catal. Sci. Technol.* 3 (2013) 2357–2364.
- [30] J. Wang, Z. Liu, G. Feng, L. Chang, W. Bao, *Fuel* 109 (2013) 101–109.
- [31] H.W. Jen, J.W. Girard, G. Cavataio, M.J. Jagner, SAE Paper 2008-01-2488, 2008.
- [32] G. Cavataio, H.W. Jen, J.W. Girard, D. Dobson, J.R. Warner, C.K. Lambert, SAE Paper 2009-01-0627, 2009.
- [33] X. Chen, N. Currier, A. Yezerets, K. Kamasamudram, SAE Paper 2013-01-1065, 2013.
- [34] I. Lezcano-Gonzalez, U. Deka, H.E. van der Bij, P. Paalanen, B. Arstad, B.M. Weckhuysen, A.M. Beale, *Appl. Catal. B: Environ.* 154/155 (2014) 339–349.
- [35] J. Wang, D. Fan, T. Yu, J. Wang, T. Hao, X. Hu, M. Shen, W. Li, *J. Catal.* 322 (2015) 84–90.
- [36] T. Yu, J. Wang, Y. Huang, M. Shen, W. Li, J. Wang, *ChemCatChem* 6 (2014) 2074–2083.
- [37] T. Yu, J. Wang, M. Shen, J. Wang, W. Li, *J. Chem. Eng.* 264 (2015) 845–855.
- [38] C. Ge, L. Liu, X. Yao, C. Tang, F. Gao, L. Dong, *Catal. Sci. Technol.* 3 (2013) 1547–1557.
- [39] R. Zhang, D. Shi, Y. Zhao, B. Chen, J. Xue, X. Liang, Z. Lei, *Catal. Today* 175 (2011) 26.
- [40] A. Lewera, P.J. Barczuk, K. Skorupska, K. Miecznikowski, M. Salamonczyk, P.J. Kulesza, *J. Electroanal. Chem.* 662 (2011) 93–99.
- [41] S. Shimizu, H. Noritake, T. Koitaya, K. Mukai, S. Yoshimoto, J. Yoshinobu, *Surf. Sci.* 608 (2013) 220–225.
- [42] A.R. Vaccaro, G. Mul, J. Pérez-Ramírez, J.A. Moulijn, *Appl. Catal. B: Environ.* 46 (2003) 687–702.